

## Constraining the Diffusion Coefficient and Cosmic-Ray Acceleration Efficiency using Gamma-ray Emission from the Star-Forming Region RCW 38

PAARMITA PANDEY <sup>1,2</sup>, LAURA A. LOPEZ <sup>1,2</sup>, ANNA L. ROSEN <sup>3,4</sup>, TODD A. THOMPSON <sup>1,2</sup>, TIM LINDEN <sup>5</sup> AND IAN BLACKSTONE <sup>6,2</sup>

<sup>1</sup>*Department of Astronomy, The Ohio State University, 140 W. 18th Ave., Columbus, OH 43210, USA*

<sup>2</sup>*Center for Cosmology and Astroparticle Physics, The Ohio State University, 191 W. Woodruff Ave., Columbus, OH 43210, USA*

<sup>3</sup>*Department of Astronomy, San Diego State University, San Diego, CA 92182, USA*

<sup>4</sup>*Computational Science Research Center, San Diego State University, San Diego, CA 92182, USA*

<sup>5</sup>*Stockholm University and The Oskar Klein Centre for Cosmoparticle Physics, Alba Nova, 10691 Stockholm, Sweden*

<sup>6</sup>*Department of Physics, Ohio State University, 191 W. Woodruff Ave, Columbus, OH 43210*

### ABSTRACT

Stellar winds from massive stars may be significant sources of cosmic rays (CRs). To investigate this connection, we report a detailed study of gamma-ray emission near the young Milky Way star cluster ( $\approx 0.5$  Myr old) in the star-forming region RCW 38 and compare this emission to its stellar wind properties and diffuse X-ray emission. Using 15 years of Fermi-LAT data in the 0.2 – 300 GeV band, we find a significant ( $\sigma > 22$ ) detection coincident with the star cluster, producing a total  $\gamma$ -ray luminosity (extrapolated over 0.1 – 500 GeV) of  $L_\gamma = (2.66 \pm 0.92) \times 10^{34}$  erg s<sup>-1</sup> adopting a power-law spectral model ( $\Gamma = 2.34 \pm 0.04$ ). Using an empirical relationship and Starburst99, we estimate the total wind power to be  $8 \times 10^{36}$  erg s<sup>-1</sup>, corresponding to a CR acceleration efficiency of  $\eta_{\text{CR}} \simeq 0.4$  for an assumed diffusion coefficient consistent with  $D = 10^{28}$  cm<sup>2</sup> s<sup>-1</sup>. Alternatively, a lower acceleration efficiency of 0.1 can produce this  $L_\gamma$  if the diffusion coefficient is smaller,  $D \simeq 2.5 \times 10^{27}$  cm<sup>2</sup> s<sup>-1</sup>. Additionally, we analyze Chandra X-ray data from the region and compare the hot-gas pressure to the CR pressure. We find the former is four orders of magnitude greater, suggesting that the CR pressure is not dynamically important relative to stellar winds. As RCW 38 is too young for supernovae to have occurred, the high CR acceleration efficiency in RCW 38 demonstrates that stellar winds may be an important source of Galactic CRs.

*Keywords:* Galactic cosmic rays (567), Gamma-ray astronomy (628), Young star clusters (1833), Stellar winds (1636), Stellar feedback (1602), X-ray sources (1822)

### 1. INTRODUCTION

Cosmic rays (CR) are relativistic charged particles that are a fundamental component of the Galaxy. CRs have a direct influence on the thermodynamics and chemistry of the interstellar and circumgalactic medium (Boulares & Cox 1990; Zweibel 2013; Padovani et al. 2020). They contribute to the ionization and heating in molecular clouds where UV and X-ray photons are shielded (Dalgarno 2006), and CR spallation is the primary mechanism of production of light elements such as Li, Be, and B (Fields & Olive 1999; Fields et al. 2000; Ramaty et al. 1997). On galactic scales, the role of CRs

in galaxy formation has received increased attention in recent years (Ruszkowski et al. 2017; Chan et al. 2019; Hopkins et al. 2020). In particular, galaxy formation simulations show that CR feedback may play a vital role in the launching of galactic-scale winds (Booth et al. 2013; Salem & Bryan 2014; Pakmor et al. 2016; Simpson 1983; Jacob et al. 2018; Modak et al. 2023) and alter the phase structure of the circumgalactic medium (e.g., Salem et al. 2016; Butsky et al. 2023).

In order to model CR feedback in galaxies, it is crucial to constrain CR acceleration and transport observationally. CR electrons are detectable at radio and X-ray wavelengths, but it is critical to probe CR protons as they comprise the bulk of the CR energy. Fortunately, emission associated with CR protons is observable with

$\gamma$ -ray facilities: when CR protons collide with gas, neutral pions are produced that decay and dominate the GeV emission of star-forming galaxies (e.g., in the Milky Way: Strong et al. 2010).

The origin of galactic CRs is a subject of ongoing discussion. Diffusive shock acceleration (DSA) in supernova remnants (SNRs) has long been considered the primary source of galactic CRs (Baade & Zwicky 1934; Drury et al. 1994; Blasi 2013). However, there is increasing evidence showing that stellar wind feedback from young massive star clusters (YMCs) may also contribute to the high-energy CR budget of star-forming galaxies (Aharonian et al. 2019). First recognized as possible CR accelerators in the 1980s (Casse & Paul 1980; Cesarsky & Montmerle 1983), particles may be accelerated either in the immediate vicinity of the stars through the shocks produced by collisions of individual stellar winds, through the reverse shock of collective winds interacting with the surrounding medium, or the forward shock at the front of the expansion in superbubbles (Parizot et al. 2004; Bykov 2014; Gupta et al. 2018a,b).

Since the advent of modern GeV and TeV facilities, several star clusters have now been detected in  $\gamma$ -rays: e.g., the Cygnus cocoon (Ackermann et al. 2011; Aharonian et al. 2019; Astiasarain et al. 2023), Westerlund 2 (Yang et al. 2018), NGC 3603 (Yang & Aharonian 2017) and (Saha et al. 2020), M17 (Liu et al. 2022), W40 (Sun et al. 2020), and W43 (Yang & Wang 2020). There are many more known YMCs in the Milky Way (see Portegies Zwart et al. 2010), a majority of which do not have reported  $\gamma$ -ray detections yet. One reason is that most of these sources are located within the Galactic plane, and it is challenging to confirm  $\gamma$ -ray associations in crowded regions due to the limited spatial resolution at GeV energies. YMCs with ages  $< 3$  Myr without nearby SNRs or pulsars are especially valuable targets to evaluate the efficacy of stellar winds as CR accelerators because these YMCs are too young for supernovae to have occurred.

In this paper, we present the Fermi Gamma-ray Space Telescope detection of the star-forming region RCW 38. Positioned one degree south of the Galactic plane and with an estimated age of 0.1 – 0.5 Myr (Wolk et al. 2006; Fukui et al. 2016), it is an optimal target to search for  $\gamma$ -rays and constrain the efficiency of CR acceleration from the collective stellar winds in a YMC.

RCW 38 is located 1.7 kpc away and is powered by an embedded (extinction coefficient  $A_V \sim 10$  mag) star cluster (Wolk et al. 2006). There are two defining IR sources in RCW 38; the brightest source at 2  $\mu\text{m}$  is IRS 2 corresponds to an O5.5 binary located at its center (DeRose et al. 2009). The brightest source at 10  $\mu\text{m}$  is IRS 1, a dust ridge that extends 0.1 –

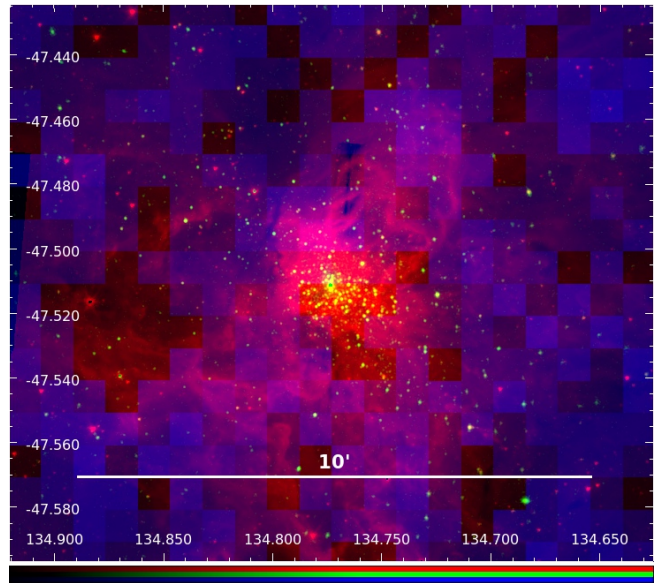


**Figure 1.** Multiwavelength image of RCW 38, with 3.6  $\mu\text{m}$  IR Spitzer image in red (Wolk et al. 2006), the Chandra X-ray broad-band (0.5 – 7.0 keV) in green, and the background subtracted 2 – 300 GeV Fermi-LAT counts map in blue. The  $\gamma$ -ray emission region is coincident with the IR and X-ray emission.

0.2 pc in the north-south direction (Wolk et al. 2006; Kuhn et al. 2015a,b). CO observations found a total cloud mass of  $2.3 \times 10^4 M_\odot$  (Fukui et al. 2016) and that the star cluster likely formed via a cloud-cloud collision, making it the third identified YMC in the Milky Way formed this way (the others being NGC 3603 (Fukui et al. 2014) and Westerlund 2 (Furukawa et al. 2009; Ohama et al. 2010)). Mužić et al. (2017) performed an extensive study of the low-mass stellar content in RCW 38’s star cluster using NACO/VLT data and found it has a top-heavy initial mass function (IMF) that is shallower than a Salpeter IMF (Salpeter 1955) or a Kroupa IMF (Kroupa 2001), with  $dN/dM \propto M^{-\alpha}$ , where  $\alpha = 1.60 \pm 0.13$ . Within the central few parsecs, the region harbors  $\sim 10^4$  stars, 20 of which are confirmed O-type stars (and nearly 30 total candidates) (Wolk et al. 2006; Broos et al. 2013; Kuhn et al. 2015b).

The Fermi-LAT data above 1 GeV from RCW 38 has been previously studied by Peron et al. (2024) and Ge et al. (2024). Both papers suggest that the observed GeV emission is caused by the interaction of CR protons accelerated by the stellar winds with the ambient gas. This paper considers the Fermi-LAT data from 0.2 – 300 GeV as well, expanding upon the previous work of by estimating the wind luminosity from observations (rather than adopting a fiducial value) and taking ad-

vantage of the Chandra X-ray data toward RCW 38 to explore the relationship between the hot gas and CRs. Specifically, we use an empirical relation between bolometric luminosity, mass-loss rate, and stellar wind velocity of the stars in RCW 38 to estimate the fraction of the energy injected by stellar winds is responsible for accelerating CRs. We then compare our estimate with that of simulated results by Starburst99. Our work focuses primarily on the observational signatures of stellar wind feedback in young clusters with an emphasis on connecting current theoretical predictions to observational analysis.

This paper is organized as follows. We present the Fermi  $\gamma$ -ray analysis in Section 2.1, including spatial and likelihood analysis confirming the association with RCW 38 (Section 2.1.1 and Section 2.1.2). We find evidence that the  $\gamma$ -ray emission is extended in Section 2.1.3, and we produce the  $\gamma$ -ray spectral energy distribution (SED) and estimate the  $\gamma$ -ray luminosity in Section 2.1.4. In Section 2.2, we analyze archival Chandra X-ray data toward RCW 38 in order to measure the hot-gas properties produced by the stellar winds in the region. In Section 3.1, we evaluate the bolometric luminosity and wind power of the region. In Section 3.2, we argue that if the gamma-ray emission is hadronic and if the CR losses are dominated by diffusion, then the observations necessitate either a high CR acceleration efficiency or a relatively small diffusion coefficient relative to typical ISM values. In Section 3.3, we find that the CR pressure is likely much weaker than the hot gas pressure, indicating that CR pressure is not dynamically important on the size scales of YMCs and their surrounding HII regions. In Section 3.4, we show that CR leptons are not likely to contribute to the detected  $\gamma$ -ray flux thereby confirming the observed  $\gamma$ -ray emission originates from the destruction of CR protons. In Section 3.5, we compare and contrast our work with that previously conducted by Peron et al. (2024) and Ge et al. (2024) on RCW 38. In Section 4, we summarize our conclusions.

## 2. DATA ANALYSIS AND RESULTS

### 2.1. Fermi-LAT Data Analysis

We used data from the Fermi  $\gamma$ -ray Space Telescope, which was launched in 2008 and houses two scientific instruments, the Large Area Telescope (LAT) and the Gamma-ray Burst Monitor (GBM). LAT onboard Fermi observes  $\gamma$ -ray photons utilizing electron-positron pair production in a silicon tracker and detects  $\gamma$ -rays in the energy range 0.1–300 GeV. It has a spatial resolution of  $< 1^\circ$  for  $E > 1$  GeV, a very wide field of view ( $\sim 2.4$  sr), and an effective area  $> 8000$  cm<sup>2</sup> (Atwood

et al. 2009). The latest upgrade to the event reconstruction process and instrumental response functions (referred to as Pass 8) improved the effective area, the accuracy of point spread function, and the system’s ability to reject cosmic-ray backgrounds (Atwood et al. 2013).

#### 2.1.1. Spatial Analysis

In our analysis, we utilized nearly 15 years of data spanning from August 8, 2008 (MET 239846401) to June 5, 2023 (MET 707616005) of LAT events in the reconstructed energy range from 200 MeV to 300 GeV within a  $20^\circ$  region of interest (ROI) at the optical coordinates of RCW 38 (R.A. =  $134.773^\circ$ , Dec =  $-47.5109^\circ$ ). We analyzed the data using Fermitools analysis package (v11r5p3<sup>1</sup>), and we evaluated the extension and spectral energy distribution of the source using the FermiPy python package (Wood et al. 2017).

We used *gtselect* to select photons of energies 200 MeV – 300 GeV with an arrival direction  $< 90^\circ$  from the local zenith to remove contamination from  $\gamma$ -rays produced by CR interactions in the upper layers of Earth’s atmosphere. The good time intervals (GTIs) when the telescope was operating normally were selected using the filters “DATA QUAL  $> 0$ ” and “LAT CONFIG==1”. The P8R3\_SOURCE\_V3 instrument response was used for analysis.

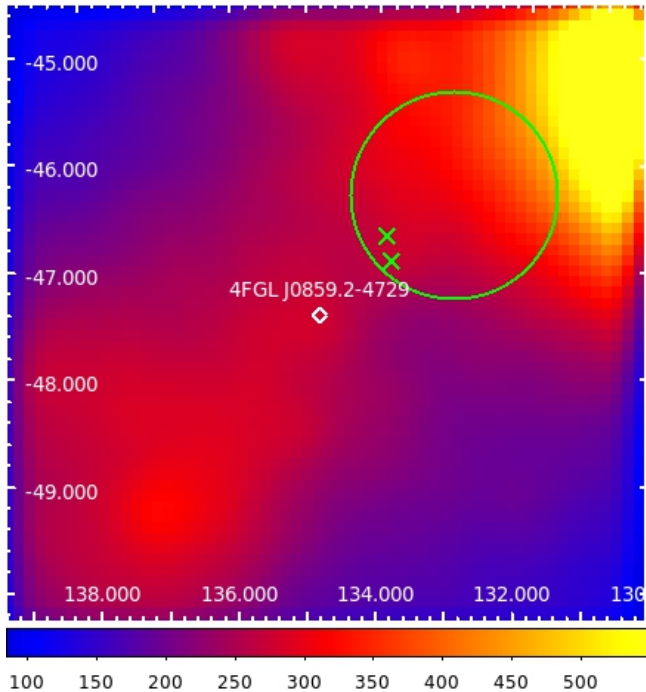
We performed a binned maximum-likelihood analysis to estimate the best-fit model parameters using a  $20^\circ$  square region centered on RCW 38 with ten equally spaced logarithmic bins in energy. We selected events only belonging to the SOURCE class (evclass=128) and evtype=3 (corresponding to standard analysis in Pass 8) within the ROI. We incorporated the Galactic and extragalactic diffuse emission and isotropic background emission in the model via the templates *gll\_iem\_v07* and *iso\_P8R3\_SOURCE\_V6\_v06* (tilt fit has not been considered). The  $\gamma$ -ray data were modeled with the comprehensive Fermi-LAT source catalog, 4FGL-DR3 (Abdollahi et al. 2022).

Figure 1 shows the 2–300 GeV background subtracted Fermi count map in blue (produced using *gtbin*) in the vicinity of RCW 38 compared to the Spitzer  $3.6\mu\text{m}$  in red (Winston et al. 2012) and the Chandra broad-band (0.5 – 7.0 keV) X-rays in green. The 68% confidence interval of the spatial resolution of the LAT is  $\approx 0.6^\circ$  at 2 GeV and  $\approx 0.1^\circ$  at 100 GeV, compared to a resolution of  $\sim 3^\circ$  at 200 MeV<sup>2</sup>. Thus, we consider the 2–300 GeV emission for spatial analysis and multiwavelength comparison, and we find the gamma-rays are spatially co-

<sup>1</sup> <https://github.com/fermi-lat/Fermitools-conda>

<sup>2</sup> [slac.stanford.edu/exp/glast/groups/canda/lat.Performance.htm](http://slac.stanford.edu/exp/glast/groups/canda/lat.Performance.htm)





**Figure 2.** Counts map of the  $6^\circ \times 6^\circ$  region centered on 4FGL J0859.2-4729 in the 0.2 – 300 GeV band. The green circle shows the extension of the Vela Jr supernova remnant. The two Xs show the position of PSR J0855-4644 and PSR J0855-4658 which are present within  $1^\circ$  of J0859.2-4729.

incident with the point sources and diffuse emission detected in the IR and X-rays.

### 2.1.2. Likelihood analysis

We employed the maximum likelihood technique to investigate the  $\gamma$ -ray emission quantitatively. The FermiTools command *glike* computes the best-fit parameters by maximizing the joint probability of getting the observed data from the input model, given a specified model for the distribution of gamma-ray sources on the sky and their spectra. The likelihood  $\mathcal{L}$  is the likelihood that our spatial and spectral model accurately captures the data. The test statistic (TS) is defined as  $\text{TS} = -2 \ln(\mathcal{L}_0/\mathcal{L}_1)$ , where  $\mathcal{L}_0$  and  $\mathcal{L}_1$  are the likelihoods without and with the addition of a source at a given position, respectively.

We used *glike* to run a binned likelihood analysis over the energy range of 200 MeV – 300 GeV. The spectral indices and normalizations of the sources within  $6^\circ$  of the source, together with the normalization of the Galactic diffuse emission and isotropic component, were free parameters in the fit. Any sources located beyond a radius of  $6^\circ$  from the target and those with significance

less than  $5\sigma$  were fixed to the spectral parameter values given in 4FGL-DR3<sup>3</sup>.

The source 4FGL J0859.2–4729 is located only  $0.03^\circ$  away from the optical coordinates of RCW 38, and thus it is a possible  $\gamma$ -ray counterpart to the star-forming region. From the 4FGL catalog, this source is not variable, and its initial TS is 495 using a log-parabola (LP) spectral model in 4FGL-DR3. There are  $\approx 800$  Fermi 4FGL sources within  $\pm 2^\circ$  of the galactic plane (Ballet et al. 2023). The probability that a random source is within  $0.03^\circ$  of the star cluster is  $\frac{0.03^2}{1500} \simeq 6 \times 10^{-7}$ . Consequently, we get the probability that one of the sources is coincident is  $\simeq 5 \times 10^{-4}$ . Thus, we interpret that this 4FGL source is likely associated with RCW 38.

According to the Australia Telescope National Facility (ATNF) Pulsar Catalog (Manchester et al. 2005), two pulsars, PSR J0855–4644 and PSR J0855–4658, are located within  $1^\circ$  of RCW 38. Fermi-LAT pulsars are frequently classified as exhibiting either a power-law or a power-law with a spectral cutoff spectrum, usually having a cutoff at energies below 10 GeV (Abdo et al. 2013). Although we cannot discard the possibility that the observed  $\gamma$ -ray emission originates from the pulsars, it appears improbable, given that a considerable amount of the emission is recorded  $> 10$  GeV range (see Fig 4). Ge et al. (2024) state that PSR J0855–4658 could not contribute  $\gamma$ -ray emission due to its low spin-down power, and PSR J0855–4658’s location  $0.8^\circ$  away from the  $\gamma$ -ray peak make it unlikely as the only source as well. It is plausible that these pulsars may contribute non-negligibly to the total  $\gamma$ -ray emission. Although the Vela Jr supernova remnant and the Vela X pulsar are bright and in the ROI, they are  $\sim 1.68^\circ$  and  $\sim 4.61^\circ$  away, respectively, sufficiently far for the Fermi PSF to resolve them. Figure 2 highlights the spatial distribution of  $\gamma$ -ray emission in the 0.2 – 300 energy band including a  $6^\circ \times 6^\circ$  region centered on 4FGL J0859.2–4729. The two pulsars are denoted by X, whereas the green circle denotes the Vela Jr supernova remnant. Both are spatially offset from the peak of the 4FGL source’s  $\gamma$ -ray emission.

To investigate the association of the 4FGL source with RCW 38 and the inherent distribution of accelerated particles, we modeled the  $\gamma$ -ray spectrum of 4FGL J0859.2–4729. In our maximum likelihood analysis, we tested a power-law (PL) and a LP spectral model. The PL model is defined as

$$\frac{dN(E)}{dE} = N_0 \left( \frac{E}{E_p} \right)^{-\Gamma}, \quad (1)$$

<sup>3</sup> [readme\\_make4FGLxml.txt](#)

where  $\Gamma$  is the spectral index,  $N_0$  is the pre-factor index (with units of  $\text{ph cm}^{-2} \text{s}^{-1} \text{MeV}^{-1}$ ), and  $E_p$  is the pivot energy, which is the energy at which error on differential flux is minimal. The LP model is defined as

$$\frac{dN(E)}{dE} = N_0 \left( \frac{E}{E_p} \right)^{-(\alpha + \beta \log \frac{E}{E_p})}, \quad (2)$$

where  $N_0$  is the pre-factor index (with units of  $\text{ph cm}^{-2} \text{s}^{-1} \text{MeV}^{-1}$ ), and  $\alpha$  and  $\beta$  are the spectral index and curvature parameter, respectively.

The results of the likelihood analysis for the two different models of 4FGL J0859.2–4729 (i.e., adopting the 4FGL-DR3 position) are listed in Table 1. Relative to the 4FGL-DR3 TS value of 495 for a LP model, a PL gives TS of 509 corresponding to a  $\sigma > 22$  significance detection in the 200 MeV – 300 GeV band. We obtain a  $\Delta\text{TS} = 15.1$  for the PL model, where  $\Delta\text{TS}$  is the improvement in log-likelihood relative to the model in the 4FGL-DR3 catalog. By comparison, the LP and PL models located at the optical coordinates of RCW 38 had  $\Delta\text{TS} = -2.4$  and  $\Delta\text{TS} = 12$ . Given that a PL model has a higher likelihood value for 4FGL J0859.2–4729 and carries one less degree of freedom with respect to the LP model, we conclude that the best characterization for the  $\gamma$ -ray emission that is coincident with RCW 38 is a PL spectrum.

To localize the  $\gamma$ -ray emission further, we produced a TS map of the 2–300 GeV emission using the command *gttmap*, which computes the improvement in likelihood if a point source is added to each spatial bin. To produce this TS map, we adopted the best-fit model output by *gtlike*, removed the source associated with RCW 38, and then computed the TS value for  $0.05^\circ$  pixels.

Figure 3 gives the TS map of RCW 38 in the 2–300 GeV band, with green contours reflecting the distribution of  $3.6\mu\text{m}$  emission observed by Spitzer (Winston et al. 2012). The greatest TS value of  $\approx 13$  in the central two pixels is coincident with the star cluster powering RCW 38 and corresponds to a  $3.6\sigma$  detection in the 2–300 GeV band.

### 2.1.3. Extension Analysis

To investigate whether 4FGL J0859.2–4729 is a point source or is extended, we conducted extension tests in FermiPy utilizing the `GTAnalysis.extension` method. We also perform a simultaneous fit to the source position. We explored two spatial models, *Radial disk* and a *Radial Gaussian*, that have symmetric, two-dimensional shapes, where the radius  $R$  and the width  $\sigma$  parameters dictate the size of the source. In both cases,

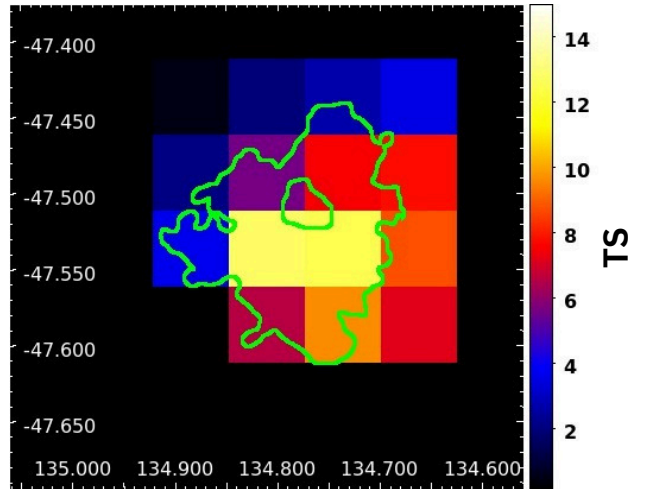


**Figure 3.** TS map of the 2 – 300 GeV band centered on RCW 38 with a pixel size of  $0.05^\circ \times 0.05^\circ$ . The green contours reflect the distribution of the  $3.6\mu\text{m}$  emission of the star-forming region observed by Spitzer (Winston et al. 2012), with the inner contour showing the extent of the star cluster powering RCW 38. The maximum TS value of  $\approx 13$  in the central two pixels is spatially coincident with the star cluster and corresponds to a  $\approx 3.6\sigma$  detection in the 2 – 300 GeV band.

we adopted the PL spectral model. When determining the optimal spatial extension for both templates, we let the galactic and isotropic backgrounds be free parameters. We also let the normalizations of sources within  $6^\circ$  of the target be free. We found that the best fit corresponds to a spatial template of a Radial Gaussian with extension size of  $\sigma = 0.24^\circ \pm 0.04^\circ$  for 4FGL J0859.2–4729 with a  $\Delta\text{TS} = 35$  ( $\approx 6\sigma$  improvement) relative to the point source spatial model. The new best-fit position for 4FGL J0859.2–4729 is R.A. =  $134.804^\circ$ , Dec =  $-47.479^\circ$  as compared to the previous position of R.A. =  $134.804^\circ$ , Dec =  $-47.488^\circ$ .

### 2.1.4. Spectral Analysis

To produce the spectral energy distribution (SED) of the  $\gamma$ -ray emission of 4FGL J0859.2–4729 using the PL spectral model and Radial Gaussian spatial distribution (see Section 2.1.3), we consider data from the energy range of 0.2 – 300 GeV, which was then used to extrapolate the 0.1 – 500 GeV total  $\gamma$ -ray luminosity. We estimated the SED by varying the normalization of the PL model independently in 8 energy bins spaced uniformly in log space from 0.2–300 GeV. Figure 4 shows the integrated gamma-ray spectrum with the errors plotted for each data point and the best-fit PL model overplotted. Photons were not detected in the two highest-energy bins above 40 GeV, so the  $2\text{-}\sigma$  upper limit for those bins is given.

**Table 1.** List of different models used for spectral and spatial analysis and their corresponding Log-likelihood values.

| Source Position                | Spectral Model | Source Type     | $\Delta\text{TS}^b$ |
|--------------------------------|----------------|-----------------|---------------------|
| 4FGL J0859.2-4729 <sup>a</sup> | Log-Parabola   | Point source    | –                   |
| 4FGL J0859.2-4729              | Power-law      | Point source    | 15.1                |
| Optical coordinates            | Log-Parabola   | Point source    | –2.3                |
| Optical coordinates            | Power-law      | Point source    | 11.0                |
| 4FGL J0859.2-4729              | Power-Law      | Radial Disk     | 27 <sup>c</sup>     |
| 4FGL J0859.2-4729              | Power-law      | Radial Gaussian | 35 <sup>c</sup>     |

<sup>a</sup>This model is from the 4FGL-DR3 catalog, yielding a TS = 495 and a log-likelihood of –16624147.3.

<sup>b</sup> $\Delta\text{TS}$  gives the improvement in log-likelihood relative to the model in the 4FGL-DR3 catalog.

<sup>c</sup> $\Delta\text{TS}$  gives the improvement in log-likelihood for the best-fit model for extension relative to the no-extension (point-source) scenario.

Figure 4 shows the integrated gamma-ray spectrum with the errors plotted for each data point and the best-fit PL model overplotted. Photons were not detected in the two highest-energy bins above 40 GeV, so a  $2\text{-}\sigma$  upper limit for that bin is given. After performing the spectral analysis, we find a best-fit photon index  $\Gamma$  in the PL spectral model to be  $\Gamma = 2.34 \pm 0.04$ , producing a total photon flux in the 0.1 – 500 GeV range of  $\Phi_{\gamma}^{>100\text{MeV}} = (2.35 \pm 0.17) \times 10^{-8}$  ph cm<sup>-2</sup> s<sup>-1</sup>. Assuming a distance of 1.7 kpc to RCW 38, the associated energy flux corresponds to a luminosity of  $L_{\gamma} = (2.66 \pm 0.92) \times 10^{34}$  erg s<sup>-1</sup>.

## 2.2. Chandra X-ray Data Analysis

To determine the properties of the hot ( $\sim 10^7$  K), diffuse gas produced by the shock-heating from stellar winds, we analyzed archival Chandra X-ray observations of RCW 38. Specifically, we used these data to check the spatial extension of RCW 38 and to compute the temperature  $kT$ , electron density  $n_e$ , pressure  $P_X$ , and X-ray luminosity ( $L_X$ ) based on the thermal bremsstrahlung continuum emission. These values are employed in Section 3 to derive the effective number density of nucleons  $n_{\text{eff}}$  and to compare to the CR pressure  $P_{\text{CR}}$  in Section 3.3.

RCW 38 was observed by Chandra four times totaling 190 ks with the ACIS-I array: for 97 ks in December 2001 (ObsID 2556), for 15 and 40 ks in June 2015 (ObsIDs 16657 and 17681, respectively), and for 38 ks in August 2015 (ObsID 17554). These data were downloaded from the Chandra archive and reduced using the Chandra Interactive Analysis of Observations CIAO version 4.14 (Fruscione et al. 2006). Data were reprocessed (us-

ing the *repro* command), combined, and exposure corrected (using the *merge\_obs* function).

Figure 1 shows the exposure-corrected, broad-band (0.5–7.0 keV) Chandra image in green, with hundreds of apparent point sources (as identified by Wolk et al. 2006). To map the diffuse X-ray emission and measure its extent, point sources were identified (using the *wavdetect* function) and removed (using the *dmfilth* command). Figure 5 shows the resulting diffuse hard X-ray (2.0–7.0 keV) map that has an angular extent of  $\approx 2.5'$  and is dominated by non-thermal emission (based on our spectral fits described below and results from Wolk et al. 2002 and Wolk et al. 2006). The centrally enhanced region corresponds to the location of the O5.5 binary in IRS 2 (DeRose et al. 2009).

Figure 6 compares the Fermi  $\gamma$ -ray, Chandra X-ray, and Spitzer ( $3.6\mu\text{m}$ ) IR images of RCW 38. As noted above, the  $\gamma$ -ray emission is coincident with the star cluster seen in X-rays and the larger star-forming complex traced by the IR.

To estimate the hot gas properties of RCW 38, we extracted and modeled source X-ray spectra from a  $2'$  radius circular region, with interior point sources excluded. We subtracted background spectra from a circular region  $\approx 6'$  southwest of RCW 38 that was  $0.5'$  in radius. The background-subtracted source spectra from each observation were modeled simultaneously using XSPEC Version 12.12 (Arnaud 1996). The model included a multiplicative constant component (CONST), one absorption (PHABS) component, a power-law component (POWERLAW), and one optically thin, thermal plasma component (APEC). The CONST component was

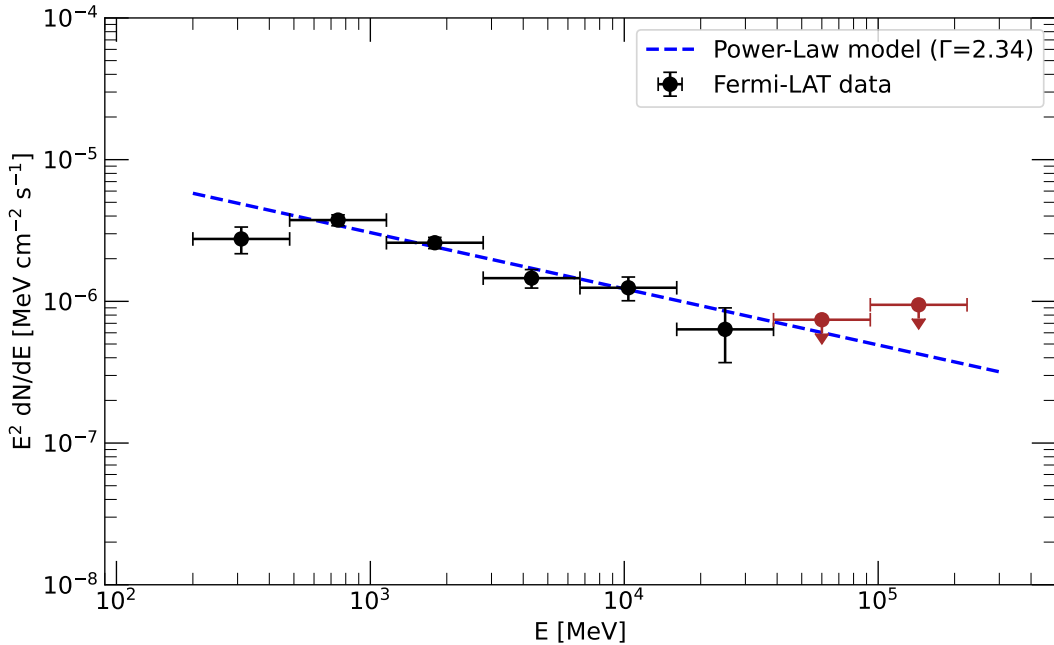


**Figure 4.** Fermi  $\gamma$ -ray SED of RCW 38. For each data point, the error bar reflects the statistical uncertainty caused by the effective area. The blue dashed line represents the best-fit PL model which has a photon index of  $\Gamma = 2.34 \pm 0.04$ . The total photon flux produced by the best-fit model in the 0.1 – 500 GeV band is  $\Phi_{\gamma}^{>100\text{MeV}} = (2.35 \pm 0.17) \times 10^{-8}$  ph cm $^{-2}$  s $^{-1}$ , corresponding to a gamma-ray luminosity of  $L_{\gamma} = (2.66 \pm 0.92) \times 10^{34}$  erg s $^{-1}$  for a distance of 1.7 kpc.

allowed to vary and accounted for slight variations in emission between the observations. The PHABS component accounted for the galactic absorption in the direction of RCW 38 and was allowed to vary. The POWERLAW component accounted for the non-thermal X-ray emission, and the APEC component represented the thermal plasma. We found that both a thermal and power-law component were necessary to adequately fit the spectra, consistent with the results of Wolk et al. (2002) and Wolk et al. (2006). We fixed abundances to solar values from Asplund et al. (2009) and photoionization cross sections from Verner et al. (1996).

The best-fit X-ray spectra are shown in Figure 7 which yielded  $\chi^2 = 1196$  with 1003 degrees of freedom (a reduced  $\chi^2 = 1.19$ ). The best-fit parameters were the following: a hydrogen column density of  $N_{\text{H}} = (1.96_{-0.06}^{+0.07}) \times 10^{22}$  cm $^{-2}$ , a hot gas temperature of  $kT = 4.52_{-0.87}^{+1.22}$  keV, and an X-ray power-law index of  $\Gamma_{\text{X}} = 2.04_{0.17}^{+0.22}$ . Nearly half ( $\approx 47\%$ ) of the emitted (unabsorbed) flux in the 0.5 – 7.0 keV band is produced by the thermal component (bremsstrahlung and line emission), with  $F_{\text{X}} = (4.4 \pm 0.5) \times 10^{-12}$  erg cm $^{-2}$  s $^{-1}$ , corresponding to an X-ray luminosity of  $L_{\text{X}} = (1.5 \pm 0.2) \times 10^{33}$  erg s $^{-1}$ .

To calculate the hot gas electron number density  $n_e$ , we used the best-fit normalization of the thermal component,  $\text{norm} = 3.25 \times 10^{-3}$  cm $^{-5}$ , which is defined as  $\text{norm} = (10^{-14} \text{EM}) / 4\pi d^2$ , where EM is the emission measure,  $\text{EM} = \int n_e n_{\text{H}} dV$ , and  $d$  is the distance to RCW 38. Relating  $n_e$  to the hydrogen number density by  $n_e = 1.2 n_{\text{H}}$  (the relation for a fully-ionized plasma that is primarily comprised of hydrogen and helium; Sarazin 1986), then  $n_e = (1.5 \times 10^{15} \text{norm } d^2 / fV)^{1/2}$ , where  $f$  is the filling factor of the hot gas and  $V$  is the hot gas volume. Assuming a spherical volume with radius  $R = 2' \approx 1$  pc and  $f = 1$ , we find  $n_e = 1.9$  cm $^{-3}$ . Assuming fully ionized hydrogen, the thermal pressure from the hot gas is given by  $P_{\text{X}} = 2n_e kT = 2.7 \times 10^{-8}$  dyn cm $^{-2}$ , which we then compare to our estimated CR pressure  $P_{\text{CR}}$  in Section 3.3.

### 3. DISCUSSION

In Section 2.1, we show that RCW 38 produces substantial  $\gamma$ -ray emission that is spatially coincident with its young star cluster. This emission may be attributed to CRs (protons and/or electrons) accelerated by the stellar winds. Due to RCW 38’s young age, no SNe have exploded in the region, making it unlikely that the  $\gamma$ -ray emission is associated with CRs accelerated by SNe.



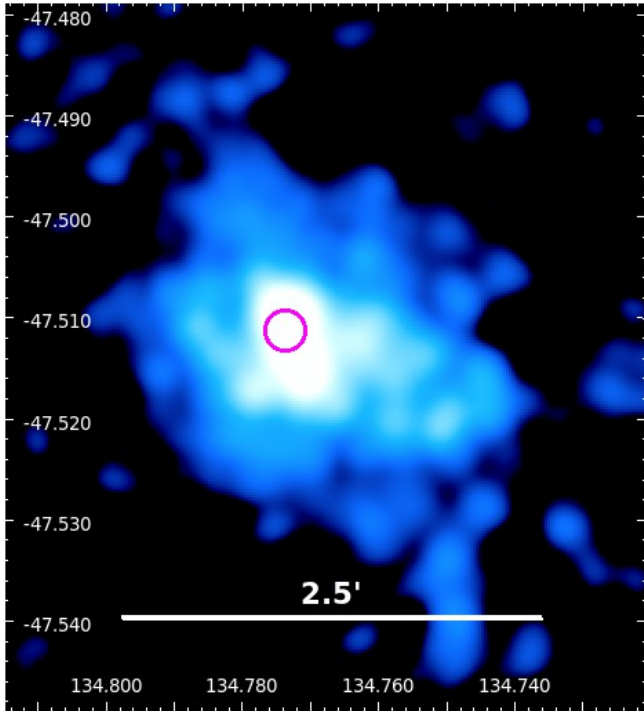


**Figure 5.** Hard X-rays (2–7 keV) from RCW 38 with point sources removed. The IRS 2 binary star system is highlighted by the magenta circle.

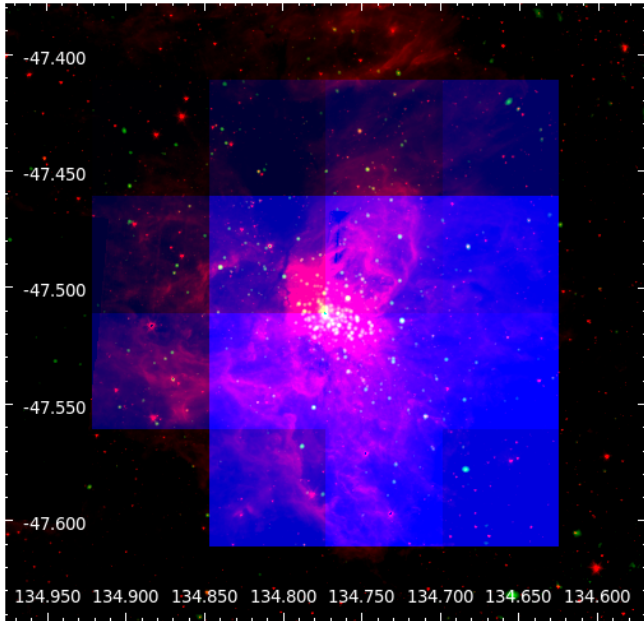


**Figure 6.** Three color image of RCW 38 combining Chandra broad-band X-ray data (green), Fermi  $\gamma$ -ray TS map of 1 degree (blue), and Spitzer infrared data (red). The  $\gamma$ -ray TS map represents the energy range of 2 – 300 GeV with 0.05-degree spatial resolution.

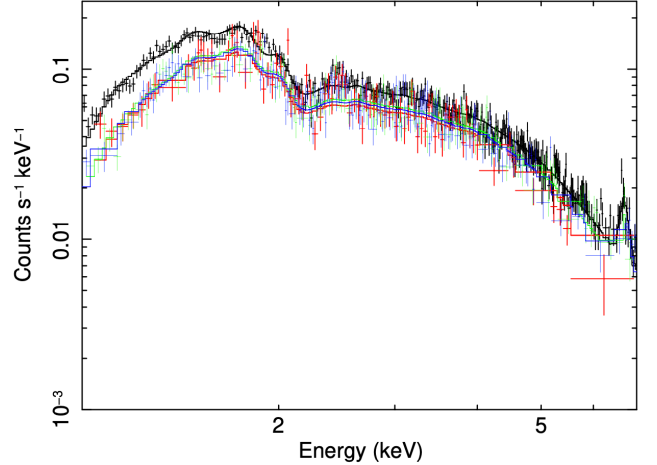


**Figure 7.** Chandra X-ray spectra of RCW 38 with the best-fit model (which included a thermal and a power-law component). The red points are the data points with error bars and the solid curves represent the best fit models. From the thermal component, we derive the properties of the hot gas, including hot gas temperature  $kT$  and electron number density  $n_e$ .

In this section, we aim to constrain the CR acceleration efficiency of the winds and the diffusion coefficient  $D$  in the star-forming region. We start by calculating the wind power of the star cluster associated with RCW 38 in Section 3.1, and then in Section 3.2, we show that in order to produce the detected  $\gamma$ -ray emission, the acceleration efficiency must be high and/or the diffusion coefficient  $D$  is small relative to value typically assumed for the nearby ISM (Strong et al. 2010). In Section 3.3, we evaluate the CR pressure and compare it to the thermal pressure  $P_X$  derived in Section 2.2. Finally, in Section 3.4, we demonstrate that the  $\gamma$ -ray emission in the region is likely due to hadronic CR losses and the observed emission is unlikely to originate from the interaction of accelerated electrons with the ambient medium.

### 3.1. Wind Power

Due to their high luminosities and large escape velocities, massive stars launch fast ( $v_w \gtrsim 10^3$  km/s), line-driven stellar winds (e.g., see reviews by Smith 2014; Vink 2022). The collective kinetic energy injection rate per massive star in a YMC is  $L_w = (1/2)\dot{M}_w v_w^2$ , where  $\dot{M}_w$  is the stellar mass-loss rate that depends on the stellar properties, such as the star’s bolometric luminosity ( $L_{\text{bol}}$ ) and surface temperature ( $T_{\text{eff}}$ ; Vink et al. 2001).

To estimate the total mechanical wind luminosity of RCW 38 (i.e.,  $L_w = (1/2)\sum_i^{N_{\text{OB}}} \dot{M}_w v_{w,i}^2$ ) we apply the



empirical relationship from [Howarth & Prinja \(1989\)](#)

$$\log_{10} \left( \dot{M}_w / M_\odot \text{ yr}^{-1} \right) = 1.69 \log_{10} (L_{\text{bol}} / L_\odot) - 15.4, \quad (3)$$

to the observed  $L_{\text{bol}}$  OB candidates from [Wolk et al. \(2006\)](#) (31 sources). We find a total YMC mass-loss rate of  $3.8 \times 10^{-6} M_\odot \text{ yr}^{-1}$  corresponding to the total  $L_{\text{bol}}$  of  $3.7 \times 10^{39} \text{ erg s}^{-1}$ .

Since the radii and masses of these sources are not constrained, we are unable to determine the expected escape speeds of the sources to estimate  $v_w$ ,  $i$  following [Vink et al. \(2001\)](#) who employ the estimate  $v_w \propto v_{\text{esc}}$ . Instead, we estimate  $v_w$  for each OB candidate identified by [Wolk et al. \(2006\)](#) in RCW 38 by applying the wind-luminosity relationship given by  $0.5 L_{\text{bol}} / c = \dot{M}_w v_w$ , which assumes that the momentum flux carried by stellar winds ( $\dot{M}_w v_w$ ) is approximately half of the radiative momentum flux ( $1/2 L_{\text{bol}} / c$ ; [Lopez et al. 2011](#); [Lancaster et al. 2021](#)). This assumption is true for YMCs, where  $L_{\text{bol}} / c$  ranges from  $(0.5 - 3) \dot{M}_w v_w$ . With these inferred  $v_w$ ,  $i$ , we estimate the total mass-loss weighted cluster wind velocity as

$$\langle v_w \rangle_{\dot{M}_w} = \frac{\sum_i^{N_{\text{OB}}} \dot{M}_{w, i} v_{w, i}}{\sum_i^{N_{\text{OB}}} \dot{M}_{w, i}}, \quad (4)$$

and obtain  $\langle v_w \rangle_{\dot{M}_w} = 2.6 \times 10^3 \text{ km s}^{-1}$ . These calculations yield a total wind luminosity of  $L_w = 8 \times 10^{36} \text{ erg s}^{-1}$  in agreement with the estimated value,  $L_w \gtrsim 3 \times 10^{36} \text{ erg s}^{-1}$ , presented in [Ge et al. \(2024\)](#).

Our estimated value for  $L_w$  is roughly an order of magnitude less than that of [Peron et al. \(2024\)](#) who assumed  $\dot{M}_w = 10^{-4} M_\odot \text{ yr}^{-1}$  and  $v_w = 1000 \text{ km s}^{-1}$ , yielding  $L_w \sim 6 \times 10^{37} \text{ erg s}^{-1}$ , following the fiducial values presented in [Cantó et al. \(2000\)](#). As a check our estimated value, we also compute this quantity from STARBURST99 ([Leitherer et al. 1999](#)). We note that since RCW 38 has a total stellar mass of  $\sim 2.5 \times 10^3 M_\odot$ , the IMF is most likely sensitive to stochastic sampling rather than being fully-sampled as expected for clusters with  $M_\star \lesssim 10^5 M_\odot$  ([da Silva et al. 2012](#)). With these caveats, we adopt the observed IMF slopes from [Mužić et al. \(2017\)](#), the total stellar mass of the cluster as  $M_{\text{tot}} = 2251 M_\odot$ , and  $40 M_\odot$  as the maximum mass of a star (see Table B1 of [Weidner et al. 2010](#)). Assuming solar metallicity, we get  $L_w = 6.79 \times 10^{36} \text{ erg s}^{-1}$ , which is comparable to our previous estimate for  $L_w$  derived using the wind momentum-luminosity relation value.

### 3.2. Cosmic-ray Injection

With  $L_w$  derived above, we now investigate the acceleration efficiency of CRs from stellar winds in RCW 38. The energy injection rate into CRs by stellar winds is

$\dot{E}_{\text{CR}} = \eta_{\text{CR}} L_w$ , where  $\eta_{\text{CR}}$  is the fraction of the wind kinetic energy that goes into accelerating primary CR protons.

Given  $\dot{E}_{\text{CR}}$ , the maximum  $\gamma$ -ray luminosity  $L_\gamma^{\text{max}}$  that can be produced by the CRs in inelastic proton-proton collisions is  $L_\gamma^{\text{max}} = f_\gamma \dot{E}_{\text{CR}}$ , where  $f_\gamma = 1/3$  represents the fraction of the energy that goes into neutral pions, which then decay to  $\gamma$ -rays. We define the calorimetry fraction  $f_{\text{cal}}$  as the ratio of the observed  $\gamma$ -ray luminosity  $L_\gamma$  to the maximum  $\gamma$ -ray luminosity  $L_\gamma^{\text{max}}$ :  $f_{\text{cal}} \equiv L_\gamma / L_\gamma^{\text{max}}$ . A low inferred value of  $f_{\text{cal}}$  can be attributed to CR escape via diffusion from the star cluster. Putting these terms together, we have

$$f_{\text{cal}} = \frac{3L_\gamma}{\eta_{\text{CR}} L_w}. \quad (5)$$

If the  $\gamma$ -rays are produced via pionic emission when CR protons collide with gas, and if the escape losses are dominated by diffusion, then  $f_{\text{cal}}$  can also constrain the ratio of those two timescales. The CR diffusion timescale  $t_{\text{diff}} \sim R^2 / D$  is of order

$$t_{\text{diff}} = 1500 \text{ yr} \left( \frac{R}{7 \text{ pc}} \right)^2 \left( \frac{10^{28} \text{ cm}^2 \text{ s}^{-1}}{D} \right), \quad (6)$$

where  $R$  is the radius of the spherical region where diffusion takes place (estimated below) and  $D$  is the diffusion coefficient normalized to a typical value in the galactic ISM ([Trotta et al. 2011](#)). From our  $\gamma$ -ray extension analysis in Section 2.1.3, RCW 38 has  $\theta \approx 0.23^\circ$ , corresponding to a physical radius of  $R = 6.8 \text{ pc}$  for a distance of  $d = 1.7 \text{ kpc}$ .

The pion loss timescale  $t_\pi$ , which corresponds to the timescale for proton-proton hadronic interaction losses, is ([Mannheim & Schlickeiser 1994](#))

$$t_\pi = 5 \times 10^4 \text{ yr} \left( \frac{n_{\text{eff}}}{10^3 \text{ cm}^{-3}} \right)^{-1}, \quad (7)$$

where  $n_{\text{eff}}$  is the effective number density of nucleons encountered by CRs (see  $n_{\text{eff}}$  estimate below). If  $t_\pi \ll t_{\text{diff}}$  and if there are no other losses (e.g., CR streaming losses), then  $f_{\text{cal}} \rightarrow 1$ . Conversely, if  $t_{\text{diff}} < t_\pi$  then  $f_{\text{cal}} \simeq t_{\text{diff}} / t_\pi$ .

Using these relations and assumptions, our estimates of  $L_w$  from Section 3.1, and our determinations of  $L_\gamma$  and  $R$  from the Fermi observations (note that the  $\gamma$ -ray extent is larger than the X-ray extent from Section 2.2 since the CR protons need to encounter dense gas before pions are produced), we can constrain  $\eta_{\text{CR}}$  and  $D$  given  $n_{\text{eff}}$ . In particular, assuming that  $f_{\text{cal}} = t_{\text{diff}} / t_\pi < 1$ , Equation 5 can be rewritten in terms of these observables:

$$\eta_{\text{CR}} \left( \frac{10^{28} \text{ cm}^2 \text{ s}^{-1}}{D} \right) \left( \frac{n_{\text{eff}}}{10^3 \text{ cm}^{-3}} \right) =$$

$$\frac{5 \times 10^4}{1500} \left( \frac{3L_\gamma}{L_w} \right) \left( \frac{7 \text{ pc}}{R} \right)^2. \quad (8)$$

Using  $L_\gamma = 2.6 \times 10^{34} \text{ erg s}^{-1}$  (Section 2.1.4) and  $L_w = 8 \times 10^{36} \text{ erg s}^{-1}$  (Section 3.1),  $3L_\gamma/L_w \simeq 0.01$ .

Finally, we estimate  $n_{\text{eff}}$ . Fukui et al. (2016) report a total gas mass in the two colliding molecular clouds associated with RCW 38 of  $2.3 \times 10^4 M_\odot$ . Assuming a spherical volume with radius  $R = 6.8 \text{ pc}$ , we find an effective number density of  $n_{\text{eff}} = 780 \text{ cm}^{-3}$ .

As an independent check, we can constrain the local gas density from our X-ray analysis. The hydrogen column density  $N_{\text{H}}$  inferred from the spectral analysis in Section 2.2 is  $N_{\text{H}} = (1.96_{-0.06}^{+0.07}) \times 10^{22} \text{ cm}^{-2}$ . If this absorbing column is due to gas in close proximity to RCW 38, then  $n_{\text{eff}} = N_{\text{H}}/R \approx 930 \text{ cm}^{-3}$ . Both estimates of  $n_{\text{eff}}$  are similar order-of-magnitude.

Adopting  $n_{\text{eff}} \sim 10^3 \text{ cm}^{-3}$ , then

$$\frac{t_\pi}{t_{\text{diff}}} \simeq 30 \left( \frac{10^3 \text{ cm}^{-3}}{n_{\text{eff}}} \right) \left( \frac{7 \text{ pc}}{R} \right)^2 \left( \frac{D}{10^{28} \text{ cm}^2 \text{ s}^{-1}} \right), \quad (9)$$

suggesting that diffusion losses dominate over pion losses for our estimated values and that Equation 8 holds.

Rewriting Equation 8 to solve for  $\eta_{\text{CR}}$ , we have

$$\eta_{\text{CR}} \simeq 0.4 \left( \frac{10^3 \text{ cm}^{-3}}{n_{\text{eff}}} \right) \left( \frac{7 \text{ pc}}{R} \right)^2 \times \left( \frac{D}{10^{28} \text{ cm}^2 \text{ s}^{-1}} \right) \left( \frac{3L_\gamma/L_w}{0.01} \right), \quad (10)$$

implying a high acceleration efficiency for stellar winds of  $\eta_{\text{CR}} \sim 0.4$  with a diffusion coefficient typical of the nearby ISM.

Alternatively, assuming the value of  $\eta_{\text{CR}} = 0.1$  which is typical of SN shocks (Vink 2012), this expression can be written as a constraint on the diffusion coefficient  $D$ :

$$D \simeq 2.5 \times 10^{27} \text{ cm}^2 \text{ s}^{-1} \left( \frac{\eta_{\text{CR}}}{0.1} \right) \left( \frac{n_{\text{eff}}}{10^3 \text{ cm}^{-3}} \right) \times \left( \frac{R}{7 \text{ pc}} \right)^2 \left( \frac{0.01}{3L_\gamma/L_w} \right). \quad (11)$$

The above scaling demonstrates that this lower CR acceleration efficiency of  $\eta_{\text{CR}} = 0.1$  necessitates a smaller diffusion coefficient of  $D \sim 2.5 \times 10^{27} \text{ cm}^2 \text{ s}^{-1}$  in the vicinity of the star cluster.

These results conform with our intuition that more rapid diffusion (escape), via either bigger  $D$  or smaller  $R$ , requires a higher CR efficiency  $\eta_{\text{CR}}$  to maintain the same observed  $\gamma$ -ray emission relative to the power provided by winds. Similarly, larger  $n_{\text{eff}}$  trades off against escape losses via the ratio  $t_\pi/t_{\text{diff}}$ . Note that for the value of  $D$  in Equation 11,  $t_\pi/t_{\text{diff}} \simeq 8$  in Equation 9,

indicating that losses are only marginally dominated by diffusion for the adopted gas density and that  $f_{\text{cal}} \simeq 0.1$ .

Overall, we see that a hadronic interpretation of the observed  $\gamma$ -ray emission passes basic checks: for  $\eta_{\text{CR}}$  in the range of  $\simeq 0.1$  and  $D \simeq 2.5 \times 10^{27} \text{ cm}^2 \text{ s}^{-1}$ , the  $\gamma$ -ray luminosity is reproduced if  $n_{\text{eff}}$  is of the order  $10^3 \text{ cm}^{-3}$ . However, if the CRs instead interact with a medium well below this nominal gas number density, the diffusion coefficient  $D$  must be proportionately smaller to maintain the same  $L_\gamma/L_w$ , as made explicit in Equations 11 and 9. We note that our constrained value of  $D$  is in accordance with theoretical estimates provided in Gupta et al. (2018b).

### 3.3. CR pressure

With these numbers and scalings in hand, the CR pressure  $P_{\text{CR}}$  in the region can be roughly estimated from

$$P_{\text{CR}} \simeq \frac{1}{3} \frac{\dot{E}_{\text{CR}} \min[t_\pi, t_{\text{diff}}]}{V}, \quad (12)$$

where  $V$  is the region's volume. Assuming again that  $t_{\text{diff}} < t_\pi$  (see Equation 9), we have that

$$P_{\text{CR}} \simeq \frac{\eta_{\text{CR}} L_w}{4\pi R D} \simeq 1 \times 10^{-12} \text{ erg cm}^{-3} \left( \frac{\eta_{\text{CR}}}{0.1} \right) \times \left( \frac{L_w}{10^{37} \text{ erg s}^{-1}} \right) \left( \frac{7 \text{ pc}}{R} \right) \left( \frac{10^{27} \text{ cm}^2 \text{ s}^{-1}}{D} \right). \quad (13)$$

We can also use Equation 8 to write  $P_{\text{CR}}$  in terms of quantities connected with observations:  $P_{\text{CR}} \simeq 3L_\gamma t_\pi / 4\pi R^3$ :

$$P_{\text{CR}} \simeq 1 \times 10^{-12} \text{ erg cm}^{-3} \left( \frac{L_\gamma}{2.6 \times 10^{34} \text{ ergs s}^{-1}} \right) \times \left( \frac{7 \text{ pc}}{R} \right)^3 \left( \frac{10^3 \text{ cm}^{-3}}{n_{\text{eff}}} \right). \quad (14)$$

These estimates are equivalent to the method of Gupta et al. (2018b).

In Section 2.2, we measured the thermal pressure of the hot gas to be  $P_{\text{X}} = 2.7 \times 10^{-8} \text{ dyn cm}^{-2}$ , roughly four orders of magnitude greater than  $P_{\text{CR}}$ . We note that the thermal pressure is calculated within a region roughly one pc in size, whereas the  $P_{\text{CR}}$  is calculated for a region seven times larger. This difference arises because the X-rays are confined to a smaller volume characterized by a decreasing density and a declining thermal pressure, as shown in Figure 1 of Gupta et al. (2018a). Our results suggest that CR feedback is most likely dynamically unimportant in very young ( $t \lesssim 0.5 \text{ Myr}$ ) YMCs. However, we note that the inferred  $P_{\text{X}}$  in RCW 38 is much larger than those estimated in  $\sim 1$ -3 Myr YMCs (e.g., see Rosen et al. 2014;

Gupta et al. 2018b). Thus, it still remains uncertain if CR feedback may be dynamically important in slightly older YMCs that contain cooler (e.g.,  $\sim 1 - 5 \times 10^6$  K) and more extended superbubbles.

### 3.4. Estimating the Leptonic $\gamma$ -ray Emission

In order to estimate if the observed  $\gamma$ -ray emission can be leptonic in origin, we evaluate the  $L_\gamma$  assuming a purely leptonic model.  $\gamma$ -ray emission can be produced via relativistic bremsstrahlung and inverse-Compton scattering of the primary CR electrons. In the latter scenario, low-energy photons such as CMB, optical, and UV (stellar radiation) can be inverse-Compton boosted by relativistic electrons to  $\gamma$ -ray energies. The energy of the scattered photons is approximately  $E_{\text{IC}} \sim \Gamma^2 E_{\text{seed}}$  where  $\Gamma$  is the Lorentz factor of the relativistic electron and  $E_{\text{seed}}$  is the energy of the seed photon (usually ranging from 0.1 – 10 eV for stellar radiation). For an optical photon of 1 eV, the Lorentz factor of the relativistic electron should be of the order of  $\sim 10^{4.5}$  such that the IC boosted  $\gamma$ -ray photon has the energy of  $\sim 1$  GeV. The timescale for inverse-Compton emission is given by

$$t_{\text{IC}}^e = \frac{\Gamma m_e c^2}{\frac{4}{3} \sigma_T c \Gamma^2 U_{\text{ph}}} \simeq 3 \times 10^6 \text{ yr} \left( \frac{10^{4.5}}{\Gamma} \right) \times \left( \frac{10^{-11} \text{ erg cm}^{-3}}{U_{\text{ph}}} \right), \quad (15)$$

where  $m_e$  is the rest mass of electron,  $\sigma_T$  is the Thomson cross-section,  $c$  is the speed of light, and  $U_{\text{ph}}$  is the stellar radiation energy density computed as  $U_{\text{ph}} \simeq (L_{\text{bol}}/4\pi r^2 c)$ . We use the values  $L_{\text{bol}} = 3.7 \times 10^{39} \text{ erg s}^{-1}$  (Section 3.1) and  $R \approx 7 \text{ pc}$  to determine  $U_{\text{ph}}$ . Note that  $t_{\text{IC}}$  is much longer than the diffusion timescale for a broad range of  $D$  (eq. 6).

Next, we estimate the  $\gamma$ -ray luminosity from IC emission. We assume that in the star-forming region, the dominant radiation field is the stellar radiation. For a given population of relativistic electrons, the number density distribution can be defined as  $n(\Gamma) = \kappa_1 \Gamma^{-p}$ , where  $p$  is the spectral index of relativistic electrons ( $p \approx 2.2$ ), and  $\kappa_1$  is the normalization constant that can be calculated from the energy density of CR electrons ( $\epsilon_{\text{CR},e}$ ) as follows (Gupta et al. 2018a):

$$\kappa_1 \approx \frac{\epsilon_{\text{CR},e}}{m_e c^2} (p-2) \left[ \frac{1}{\Gamma_{\text{min}}^{p-2}} - \frac{1}{\Gamma_{\text{max}}^{p-2}} \right]^{-1}. \quad (16)$$

The upper-limit on the inverse-Compton  $\gamma$ -ray luminosity ( $L_\gamma^{\text{IC}}$ ) can be determined by (Gupta et al. 2018a):

$$L_\gamma^{\text{IC}} = \int_V dV \left[ \frac{4}{3} \sigma_T c U_{\text{ph}} \kappa_1 \frac{\Gamma_{\text{max}}^{(3-p)} - \Gamma_{\text{min}}^{(3-p)}}{3-p} \right], \quad (17)$$

where  $V$  is the volume. We take  $\Gamma_{\text{min}} = 1$  and  $\Gamma_{\text{max}} = 10^6$ . Based on the calculations above, and assuming  $L_\gamma^{\text{IC}} \simeq L_\gamma^{\text{obs}}$ , we find that the implied value of the CR electron energy density  $\epsilon_{\text{CR},e}$  must be 1000 times higher than the CR proton energy density under the assumptions of Section 3.3. This in turn implies that for primary CR electrons, the acceleration efficiency would need to be  $\eta_{\text{CR},e} \gg 1$  (from Eqn. 13). Thus, a leptonic model where the observed  $\gamma$ -ray emission is dominated by inverse-Compton emission from primary CR electrons interacting with starlight from the cluster is strongly disfavored.

Importantly, our effective number density ( $n_{\text{eff}}$ ) estimates in Section 3.2, derived from X-ray gas density and CO observations, indicate the presence of a dense medium. If primary CR electrons are interacting with such a dense medium then relativistic bremsstrahlung will be dominant over inverse-Compton losses. To see this, note that the timescale for relativistic bremsstrahlung losses is given by (Blumenthal & Gould 1970)

$$t_{\text{brems}}^e \simeq 4 \times 10^4 \text{ yr} \left( \frac{10^3 \text{ cm}^{-3}}{n_{\text{eff}}} \right). \quad (18)$$

Note that we have used  $\Gamma \simeq 10^{4.5}$  to estimate the cooling timescale above, but the energy dependence of  $t_{\text{brems}}^e$  is weak. The relativistic bremsstrahlung loss timescale is similar to  $t_\pi$  (Eq. 7), with the same dependence on  $n_{\text{eff}}$ . The ratio of the relativistic bremsstrahlung and IC cooling timescales is  $\simeq 0.01$  (Eq. 15), suggesting that relativistic bremsstrahlung could dominate inverse-Compton emission if CR electrons interact with the average density medium.

However, if CR electrons interact with the average density medium, CR protons would too. Since we expect the CR acceleration efficiency for protons to be larger than for primary electrons  $\eta_{\text{CR},p} \gg \eta_{\text{CR},e}$ , we would thus expect pion losses from CR proton collisions with the ambient medium to dominate the observed  $\gamma$ -ray emission. Therefore, a hadronic origin for the  $\gamma$ -rays emission appears more plausible than a solely leptonic origin via either inverse-Compton or relativistic bremsstrahlung.

### 3.5. Comparison to Previous Fermi Work on RCW 38

During the completion of this manuscript, work by Peron et al. (2024) was published which provides an independent analysis of Fermi data toward several young star clusters in the Vela molecular ridge, including RCW 38. They reported  $L_\gamma(> 1 \text{ GeV}) = 5 \times 10^{33} \text{ erg s}^{-1}$  based on a power-law model with an index of  $\Gamma = 2.56 \pm 0.05$  at an assumed distance of  $d = 1.6 \text{ kpc}$ . If placed at our assumed distance of  $d = 1.7 \text{ kpc}$ , their luminosity becomes  $L_\gamma(> 1 \text{ GeV}) = 5.6 \times 10^{33} \text{ erg s}^{-1}$ , which is

comparable to our calculated value of  $L_\gamma(> 1 \text{ GeV}) = 5.2 \times 10^{33} \text{ erg s}^{-1}$  (Section 2.1.4).

Additionally, Peron et al. (2024) estimated an upper limit on the wind power from the star cluster using the Weaver et al. (1977) model that relates the observed bubble radius to wind power, ambient density, and age. They assumed a mass-loss rate of  $\dot{M} = 2 \times 10^{-4} M_\odot \text{ yr}^{-1}$ , which is higher than our estimated value  $\dot{M} = 3.8 \times 10^{-6} M_\odot \text{ yr}^{-1}$  (see Sec. 3.1). They further calculated  $\dot{E}_{\text{CR}}$  using a calorimetric assumption (i.e., all accelerated CRs lose their energy via pion decay), finding a lower limit on  $\eta_{\text{CR}}$  for RCW 38 to be  $\approx 0.004\%$  (see their Table 1). If we adopt their assumed mass-loss rate and only consider  $L_\gamma$  above 1 GeV, then we would find  $\eta_{\text{CR}}$  becomes  $\approx 0.003\%$ , similar to their value. Thus, the discrepancy in the derived  $\eta_{\text{CR}}$  values can be mostly attributed to the difference in wind luminosity estimates: their reported wind luminosity is  $\simeq 6 \times 10^{37} \text{ erg s}^{-1}$ , which is greater than our value of  $8 \times 10^{36} \text{ erg s}^{-1}$  (Sec. 3.1), leading to a much lower value of  $\eta_{\text{CR}}$ .

Ge et al. (2024) also reported the Fermi-LAT detection of RCW 38 using data above 1 GeV energy range. They reported  $L_\gamma(> 1 \text{ GeV}) = 1.6 \times 10^{33} \text{ erg s}^{-1}$  based on a power-law model with an index of  $\Gamma = 2.44 \pm 0.03$  at an assumed distance of  $d = 1.7 \text{ kpc}$ . In addition, they estimated an effective gas density in the region to be  $328 \text{ cm}^{-3}$  using the CO composite survey. This value is lower as compared to our calculated value of  $n_{\text{eff}} = 1000 \text{ cm}^{-3}$ . Using standard literature values of  $\dot{M}$  and  $v_w$ , they constrain the wind power to be  $3 \times 10^{36} \text{ erg s}^{-1}$ , which is smaller than our value of  $8 \times 10^{36} \text{ erg s}^{-1}$ . They assumed a CR acceleration efficiency of 10 percent. They derived a diffusion coefficient value of  $4 \times 10^{26} \text{ cm}^2 \text{ s}^{-1}$ , which is an order of magnitude lower than our estimated value of  $2.5 \times 10^{27} \text{ cm}^2 \text{ s}^{-1}$  (see Eqn.11), for the same CR acceleration efficiency. The discrepancy in the values can be associated with their lower estimate of the total number density of gas in the region.

Overall, the three papers agree that stellar wind feedback from YMCs produce CR protons that are detectable by Fermi.

#### 4. CONCLUSIONS

We report the significant  $\gamma$ -ray detection ( $\sigma > 22$ ) of the young ( $< 0.5 \text{ Myr}$  old) star cluster in the star-forming region RCW 38 using 15 years of Fermi-LAT data. We find that the Fermi source 4FGL J0859.2–4729 is potentially associated with the star cluster and has an angular extent of  $\approx 0.23 \pm 0.04^\circ$  (Section 2.1.2 and Section 2.1.3). The  $\gamma$ -ray SED follows a PL distribution with a photon

index of  $\Gamma = 2.34 \pm 0.04$  (Figure 4), and we estimate the luminosity to be  $L_\gamma = (2.66 \pm 0.92) \times 10^{34} \text{ erg s}^{-1}$  in the 0.1 – 500 GeV band (Section 2.1.4).

Our estimates suggest that the observed  $\gamma$ -ray emission is hadronic in origin, resulting from pion production as CR protons interact with the high-density ambient medium. Purely leptonic models via inverse-Compton or relativistic bremsstrahlung are disfavored under simple assumptions about the primary CR acceleration efficiency (Section 3.4). Given that no SNe have occurred in a star cluster of this age, the detected  $\gamma$ -ray emission likely arises from CRs accelerated by stellar winds.

We use the observed bolometric luminosity of the OB candidates in the star cluster to determine the total stellar wind luminosity of  $L_w = 8 \times 10^{36} \text{ erg s}^{-1}$  (Section 3.1). With this estimate, we constrain the CR acceleration efficiency  $\eta_{\text{CR}}$  and the diffusion coefficient  $D$  together near the star cluster. We demonstrate that the observed  $\gamma$ -ray luminosity necessitates a high CR efficiency of  $\eta_{\text{CR}} \simeq 0.4$  if the diffusion coefficient is consistent with the local ISM value of  $D = 10^{28} \text{ cm}^2 \text{ s}^{-1}$ . Alternatively, a CR efficiency of  $\eta_{\text{CR}} \simeq 0.1$  is possible if the diffusion coefficient is smaller around the region,  $D \simeq 2.5 \times 10^{27} \text{ cm}^2 \text{ s}^{-1}$  (Section 3.2; eqs. 10, 11).

We estimate a CR pressure in the region of  $P_{\text{CR}} = 1 \times 10^{-12} \text{ erg cm}^{-3}$  (Section 3.3), roughly four orders of magnitude lower than the thermal pressure of the hot gas  $P_X = 2.7 \times 10^{-8} \text{ dyn cm}^{-2}$  (Section 2.2). Our results suggest that CR feedback is dynamically less important than the thermal pressure from stellar wind feedback in RCW 38’s young cluster.

Our work adds to the growing body of literature establishing that stellar winds from YMCs contribute to the galactic CR population. Similar analyses on other YMCs would be valuable to establish how the CR acceleration, transport, and dynamics evolve with cluster properties and age.

*Software:* CIAO (v4.14; Fruscione et al. 2006), XSPEC (v12.12.1; Arnaud 1996), Fermitools (v11r5p31), FermiPy python package (Wood et al. 2017).

This paper employs a list of Chandra datasets, obtained by the Chandra X-ray Observatory, contained in the Chandra Data Collection (CDC) doi:291.



PP is grateful to Lachlan Lancaster, Biman Nath, and Jordan Eagle for their valuable input and constructive feedback. LAL acknowledges support through the Heising-Simons Foundation grant 2022-3533. LAL and LL gratefully acknowledge the support of the Simons Foundation. ALR acknowledges support from the National Science Foundation (NSF) Astronomy and Astrophysics Postdoctoral Fellowship under award AST-2202249. TAT and IB are supported in part by NASA grant 80NSSC23K1480. TL is supported by the European Research Council under grant 742104, the Swedish National Space Agency under contract 117/19 and the Swedish Research Council under contract 2022-04283.

## REFERENCES

- Abdo, A. A., Ajello, M., Allafort, A., et al. 2013, *ApJS*, 208, 17, doi: [10.1088/0067-0049/208/2/17](https://doi.org/10.1088/0067-0049/208/2/17)
- Abdollahi, S., Acero, F., Baldini, L., et al. 2022, *ApJS*, 260, 53, doi: [10.3847/1538-4365/ac6751](https://doi.org/10.3847/1538-4365/ac6751)
- Ackermann, M., Ajello, M., Allafort, A., et al. 2011, *Science*, 334, 1103, doi: [10.1126/science.1210311](https://doi.org/10.1126/science.1210311)
- Aharonian, F., Yang, R., & de Oña Wilhelmi, E. 2019, *Nature Astronomy*, 3, 561, doi: [10.1038/s41550-019-0724-0](https://doi.org/10.1038/s41550-019-0724-0)
- Arnaud, K. A. 1996, in *Astronomical Society of the Pacific Conference Series*, Vol. 101, *Astronomical Data Analysis Software and Systems V*, ed. G. H. Jacoby & J. Barnes, 17
- Asplund, M., Grevesse, N., Sauval, A. J., & Scott, P. 2009, *ARA&A*, 47, 481, doi: [10.1146/annurev.astro.46.060407.145222](https://doi.org/10.1146/annurev.astro.46.060407.145222)
- Astiasarain, X., Tibaldo, L., Martin, P., Knödlseeder, J., & Remy, Q. 2023, *A&A*, 671, A47, doi: [10.1051/0004-6361/202245573](https://doi.org/10.1051/0004-6361/202245573)
- Atwood, W., Albert, A., Baldini, L., et al. 2013, arXiv e-prints, arXiv:1303.3514, doi: [10.48550/arXiv.1303.3514](https://doi.org/10.48550/arXiv.1303.3514)
- Atwood, W. B., Abdo, A. A., Ackermann, M., et al. 2009, *ApJ*, 697, 1071, doi: [10.1088/0004-637X/697/2/1071](https://doi.org/10.1088/0004-637X/697/2/1071)
- Baade, W., & Zwicky, F. 1934, *Proceedings of the National Academy of Science*, 20, 254, doi: [10.1073/pnas.20.5.254](https://doi.org/10.1073/pnas.20.5.254)
- Ballet, J., Bruel, P., Burnett, T. H., Lott, B., & The Fermi-LAT collaboration. 2023, arXiv e-prints, arXiv:2307.12546, doi: [10.48550/arXiv.2307.12546](https://doi.org/10.48550/arXiv.2307.12546)
- Blasi, P. 2013, *A&A Rv*, 21, 70, doi: [10.1007/s00159-013-0070-7](https://doi.org/10.1007/s00159-013-0070-7)
- Blumenthal, G. R., & Gould, R. J. 1970, *Rev. Mod. Phys.*, 42, 237, doi: [10.1103/RevModPhys.42.237](https://doi.org/10.1103/RevModPhys.42.237)
- Booth, C. M., Agertz, O., Kravtsov, A. V., & Gnedin, N. Y. 2013, *ApJL*, 777, L16, doi: [10.1088/2041-8205/777/1/L16](https://doi.org/10.1088/2041-8205/777/1/L16)
- Boulares, A., & Cox, D. P. 1990, *ApJ*, 365, 544, doi: [10.1086/169509](https://doi.org/10.1086/169509)
- Broos, P. S., Getman, K. V., Povich, M. S., et al. 2013, *ApJS*, 209, 32, doi: [10.1088/0067-0049/209/2/32](https://doi.org/10.1088/0067-0049/209/2/32)
- Butsky, I. S., Nakum, S., Ponnada, S. B., et al. 2023, *MNRAS*, 521, 2477, doi: [10.1093/mnras/stad671](https://doi.org/10.1093/mnras/stad671)
- Bykov, A. M. 2014, *A&A Rv*, 22, 77, doi: [10.1007/s00159-014-0077-8](https://doi.org/10.1007/s00159-014-0077-8)
- Cantó, J., Raga, A. C., & Rodríguez, L. F. 2000, *ApJ*, 536, 896, doi: [10.1086/308983](https://doi.org/10.1086/308983)
- Casse, M., & Paul, J. A. 1980, *ApJ*, 237, 236, doi: [10.1086/157863](https://doi.org/10.1086/157863)
- Cesarsky, C. J., & Montmerle, T. 1983, *SSRv*, 36, 173, doi: [10.1007/BF00167503](https://doi.org/10.1007/BF00167503)
- Chan, T. K., Kereš, D., Hopkins, P. F., et al. 2019, *MNRAS*, 488, 3716, doi: [10.1093/mnras/stz1895](https://doi.org/10.1093/mnras/stz1895)
- da Silva, R. L., Fumagalli, M., & Krumholz, M. 2012, *ApJ*, 745, 145, doi: [10.1088/0004-637X/745/2/145](https://doi.org/10.1088/0004-637X/745/2/145)
- Dalgarno, A. 2006, *Proceedings of the National Academy of Science*, 103, 12269, doi: [10.1073/pnas.0602117103](https://doi.org/10.1073/pnas.0602117103)
- DeRose, K. L., Bourke, T. L., Gutermuth, R. A., et al. 2009, *AJ*, 138, 33, doi: [10.1088/0004-6256/138/1/33](https://doi.org/10.1088/0004-6256/138/1/33)
- Drury, L. O., Aharonian, F. A., & Voelk, H. J. 1994, *A&A*, 287, 959, doi: [10.48550/arXiv.astro-ph/9305037](https://doi.org/10.48550/arXiv.astro-ph/9305037)
- Fields, B. D., & Olive, K. A. 1999, *ApJ*, 516, 797, doi: [10.1086/307145](https://doi.org/10.1086/307145)
- Fields, B. D., Olive, K. A., Vangioni-Flam, E., & Cassé, M. 2000, *ApJ*, 540, 930, doi: [10.1086/309356](https://doi.org/10.1086/309356)

- Fruscione, A., McDowell, J. C., Allen, G. E., et al. 2006, in Society of Photo-Optical Instrumentation Engineers (SPIE) Conference Series, Vol. 6270, Society of Photo-Optical Instrumentation Engineers (SPIE) Conference Series, ed. D. R. Silva & R. E. Doxsey, 62701V, doi: [10.1117/12.671760](https://doi.org/10.1117/12.671760)
- Fukui, Y., Ohama, A., Hanaoka, N., et al. 2014, *ApJ*, 780, 36, doi: [10.1088/0004-637X/780/1/36](https://doi.org/10.1088/0004-637X/780/1/36)
- Fukui, Y., Torii, K., Ohama, A., et al. 2016, *ApJ*, 820, 26, doi: [10.3847/0004-637X/820/1/26](https://doi.org/10.3847/0004-637X/820/1/26)
- Furukawa, N., Dawson, J. R., Ohama, A., et al. 2009, *ApJL*, 696, L115, doi: [10.1088/0004-637X/696/2/L115](https://doi.org/10.1088/0004-637X/696/2/L115)
- Ge, T.-T., Sun, X.-N., Yang, R.-Z., et al. 2024, *MNRAS*, 530, 1144, doi: [10.1093/mnras/stae930](https://doi.org/10.1093/mnras/stae930)
- Gupta, S., Nath, B. B., & Sharma, P. 2018a, *MNRAS*, 479, 5220, doi: [10.1093/mnras/sty1846](https://doi.org/10.1093/mnras/sty1846)
- Gupta, S., Nath, B. B., Sharma, P., & Eichler, D. 2018b, *MNRAS*, 473, 1537, doi: [10.1093/mnras/stx2427](https://doi.org/10.1093/mnras/stx2427)
- Hopkins, P. F., Chan, T. K., Garrison-Kimmel, S., et al. 2020, *MNRAS*, 492, 3465, doi: [10.1093/mnras/stz3321](https://doi.org/10.1093/mnras/stz3321)
- Howarth, I. D., & Prinja, R. K. 1989, *ApJS*, 69, 527, doi: [10.1086/191321](https://doi.org/10.1086/191321)
- Jacob, S., Pakmor, R., Simpson, C. M., Springel, V., & Pfrommer, C. 2018, *MNRAS*, 475, 570, doi: [10.1093/mnras/stx3221](https://doi.org/10.1093/mnras/stx3221)
- Kroupa, P. 2001, *MNRAS*, 322, 231, doi: [10.1046/j.1365-8711.2001.04022.x](https://doi.org/10.1046/j.1365-8711.2001.04022.x)
- Kuhn, M. A., Feigelson, E. D., Getman, K. V., et al. 2015a, *The Astrophysical Journal*, 812, 131, doi: [10.1088/0004-637X/812/2/131](https://doi.org/10.1088/0004-637X/812/2/131)
- Kuhn, M. A., Getman, K. V., & Feigelson, E. D. 2015b, *The Astrophysical Journal*, 802, 60, doi: [10.1088/0004-637X/802/1/60](https://doi.org/10.1088/0004-637X/802/1/60)
- Lancaster, L., Ostriker, E. C., Kim, J.-G., & Kim, C.-G. 2021, *ApJ*, 914, 89, doi: [10.3847/1538-4357/abf8ab](https://doi.org/10.3847/1538-4357/abf8ab)
- Leitherer, C., Schaerer, D., Goldader, J. D., et al. 1999, *ApJS*, 123, 3, doi: [10.1086/313233](https://doi.org/10.1086/313233)
- Liu, B., Yang, R.-z., & Chen, Z. 2022, *MNRAS*, 513, 4747, doi: [10.1093/mnras/stac1252](https://doi.org/10.1093/mnras/stac1252)
- Lopez, L. A., Krumholz, M. R., Bolatto, A. D., Prochaska, J. X., & Ramirez-Ruiz, E. 2011, *ApJ*, 731, 91, doi: [10.1088/0004-637X/731/2/91](https://doi.org/10.1088/0004-637X/731/2/91)
- Manchester, R. N., Hobbs, G. B., Teoh, A., & Hobbs, M. 2005, *AJ*, 129, 1993, doi: [10.1086/428488](https://doi.org/10.1086/428488)
- Mannheim, K., & Schlickeiser, R. 1994, *A&A*, 286, 983, doi: [10.48550/arXiv.astro-ph/9402042](https://doi.org/10.48550/arXiv.astro-ph/9402042)
- Modak, S., Quataert, E., Jiang, Y.-F., & Thompson, T. A. 2023, *MNRAS*, 524, 6374, doi: [10.1093/mnras/stad2257](https://doi.org/10.1093/mnras/stad2257)
- Mužić, K., Schödel, R., Scholz, A., et al. 2017, *MNRAS*, 471, 3699, doi: [10.1093/mnras/stx1906](https://doi.org/10.1093/mnras/stx1906)
- Ohama, A., Dawson, J. R., Furukawa, N., et al. 2010, *ApJ*, 709, 975, doi: [10.1088/0004-637X/709/2/975](https://doi.org/10.1088/0004-637X/709/2/975)
- Padovani, M., Ivlev, A. V., Galli, D., et al. 2020, *SSRv*, 216, 29, doi: [10.1007/s11214-020-00654-1](https://doi.org/10.1007/s11214-020-00654-1)
- Pakmor, R., Pfrommer, C., Simpson, C. M., & Springel, V. 2016, *ApJL*, 824, L30, doi: [10.3847/2041-8205/824/2/L30](https://doi.org/10.3847/2041-8205/824/2/L30)
- Parizot, E., Marcowith, A., van der Swaluw, E., Bykov, A. M., & Tatischeff, V. 2004, *A&A*, 424, 747, doi: [10.1051/0004-6361:20041269](https://doi.org/10.1051/0004-6361:20041269)
- Peron, G., Casanova, S., Gabici, S., Baghmanyan, V., & Aharonian, F. 2024, *Nature Astronomy*, doi: [10.1038/s41550-023-02168-6](https://doi.org/10.1038/s41550-023-02168-6)
- Portegies Zwart, S. F., McMillan, S. L. W., & Gieles, M. 2010, *ARA&A*, 48, 431, doi: [10.1146/annurev-astro-081309-130834](https://doi.org/10.1146/annurev-astro-081309-130834)
- Ramaty, R., Kozlovsky, B., Lingenfelter, R. E., & Reeves, H. 1997, *ApJ*, 488, 730, doi: [10.1086/304744](https://doi.org/10.1086/304744)
- Rosen, A. L., Lopez, L. A., Krumholz, M. R., & Ramirez-Ruiz, E. 2014, *MNRAS*, 442, 2701, doi: [10.1093/mnras/stu1037](https://doi.org/10.1093/mnras/stu1037)
- Ruszkowski, M., Yang, H. Y. K., & Zweibel, E. 2017, *ApJ*, 834, 208, doi: [10.3847/1538-4357/834/2/208](https://doi.org/10.3847/1538-4357/834/2/208)
- Saha, L., Domínguez, A., Tibaldo, L., et al. 2020, *ApJ*, 897, 131, doi: [10.3847/1538-4357/ab9ac2](https://doi.org/10.3847/1538-4357/ab9ac2)
- Salem, M., & Bryan, G. L. 2014, *MNRAS*, 437, 3312, doi: [10.1093/mnras/stt2121](https://doi.org/10.1093/mnras/stt2121)
- Salem, M., Bryan, G. L., & Corlies, L. 2016, *MNRAS*, 456, 582, doi: [10.1093/mnras/stv2641](https://doi.org/10.1093/mnras/stv2641)
- Salpeter, E. E. 1955, *ApJ*, 121, 161, doi: [10.1086/145971](https://doi.org/10.1086/145971)
- Sarazin, C. L. 1986, *Reviews of Modern Physics*, 58, 1, doi: [10.1103/RevModPhys.58.1](https://doi.org/10.1103/RevModPhys.58.1)
- Simpson, J. A. 1983, *Annual Review of Nuclear and Particle Science*, 33, 323, doi: [10.1146/annurev.ns.33.120183.001543](https://doi.org/10.1146/annurev.ns.33.120183.001543)
- Smith, N. 2014, *ARA&A*, 52, 487, doi: [10.1146/annurev-astro-081913-040025](https://doi.org/10.1146/annurev-astro-081913-040025)
- Strong, A. W., Porter, T. A., Digel, S. W., et al. 2010, *ApJL*, 722, L58, doi: [10.1088/2041-8205/722/1/L58](https://doi.org/10.1088/2041-8205/722/1/L58)
- Sun, X.-N., Yang, R.-Z., Liang, Y.-F., et al. 2020, *A&A*, 639, A80, doi: [10.1051/0004-6361/202037580](https://doi.org/10.1051/0004-6361/202037580)
- Trotta, R., Jóhannesson, G., Moskalenko, I. V., et al. 2011, *ApJ*, 729, 106, doi: [10.1088/0004-637X/729/2/106](https://doi.org/10.1088/0004-637X/729/2/106)
- Verner, D. A., Ferland, G. J., Korista, K. T., & Yakovlev, D. G. 1996, *ApJ*, 465, 487, doi: [10.1086/177435](https://doi.org/10.1086/177435)
- Vink, J. 2012, *A&A Rv*, 20, 49, doi: [10.1007/s00159-011-0049-1](https://doi.org/10.1007/s00159-011-0049-1)
- Vink, J. S. 2022, *ARA&A*, 60, 203, doi: [10.1146/annurev-astro-052920-094949](https://doi.org/10.1146/annurev-astro-052920-094949)
- Vink, J. S., de Koter, A., & Lamers, H. J. G. L. M. 2001, *A&A*, 369, 574, doi: [10.1051/0004-6361:20010127](https://doi.org/10.1051/0004-6361:20010127)

- Weaver, R., McCray, R., Castor, J., Shapiro, P., & Moore, R. 1977, *ApJ*, 218, 377, doi: [10.1086/155692](https://doi.org/10.1086/155692)
- Weidner, C., Kroupa, P., & Bonnell, I. A. D. 2010, *MNRAS*, 401, 275, doi: [10.1111/j.1365-2966.2009.15633.x](https://doi.org/10.1111/j.1365-2966.2009.15633.x)
- Winston, E., Wolk, S. J., Bourke, T. L., et al. 2012, *ApJ*, 744, 126, doi: [10.1088/0004-637X/744/2/126](https://doi.org/10.1088/0004-637X/744/2/126)
- Wolk, S. J., Bourke, T. L., Smith, R. K., Spitzbart, B., & Alves, J. 2002, *ApJL*, 580, L161, doi: [10.1086/345611](https://doi.org/10.1086/345611)
- Wolk, S. J., Spitzbart, B. D., Bourke, T. L., & Alves, J. 2006, *AJ*, 132, 1100, doi: [10.1086/505704](https://doi.org/10.1086/505704)
- Wood, M., Caputo, R., Charles, E., et al. 2017, in International Cosmic Ray Conference, Vol. 301, 35th International Cosmic Ray Conference (ICRC2017), 824, doi: [10.22323/1.301.0824](https://doi.org/10.22323/1.301.0824)
- Yang, R.-z., & Aharonian, F. 2017, *A&A*, 600, A107, doi: [10.1051/0004-6361/201630213](https://doi.org/10.1051/0004-6361/201630213)
- Yang, R.-z., de Oña Wilhelmi, E., & Aharonian, F. 2018, *A&A*, 611, A77, doi: [10.1051/0004-6361/201732045](https://doi.org/10.1051/0004-6361/201732045)
- Yang, R.-Z., & Wang, Y. 2020, *A&A*, 640, A60, doi: [10.1051/0004-6361/202037518](https://doi.org/10.1051/0004-6361/202037518)
- Zweibel, E. G. 2013, *Physics of Plasmas*, 20, 055501, doi: [10.1063/1.4807033](https://doi.org/10.1063/1.4807033)